ORIGINAL ARTICLE

Cancer stem-like cells directly participate in vasculogenic mimicry channels in triple-negative breast cancer

Huizhi Sun[1], Nan Yao[1], Siqi Cheng[1], Linqi Li[1], Shiqi Liu[1], Zhao Yang[1], Guanjie Shang[1], Danfang Zhang[1,2], Zhi Yao[1,3]

[1]Department of Pathology, Tianjin Medical University, Tianjin 300070, China; [2]Department of Pathology, General Hospital of Tianjin Medical University, Tianjin 300070, China; [3]Department of Immunology, Tianjin Medical University, Tianjin 300070, China

ABSTRACT

Objective: Vasculogenic mimicry (VM) channels that are lined by tumor cells are a functional blood supply in malignant tumors. However, the role of VM-initiating cells remains poorly understood. Cancer stem-like cells (CSCs) are positively correlated with VM. In this study, triple-negative breast cancer (TNBC) enriched with CSCs was used to investigate the relationship between VM and CSCs.

Methods: The expression of several CSC markers was detected by immunohistochemistry in 100 human breast cancer samples. The clinical significance of CSC markers and the relationship between VM, CSCs, breast cancer subtypes, and VM-associated proteins were analyzed. CD133+ and ALDH+ human and mouse TNBC cells were isolated by FACS to examine the ability of VM formation and the spatial relationship between VM and CSCs.

Results: CSCs were associated with TNBC subtype and VM in human invasive breast cancer. CSCs in TNBC MDA-MB-231 cells formed more VM channels and expressed more molecules promoting VM than the non-TNBC MCF-7 cells *in vitro*. MDA-MB-231 cells that encircled VM channels on Matrigel expressed CD133. Moreover, CSCs were located near VM channels in the 3D reconstructed blood supply system in human TNBC grafts. The CD133+ and ALDH+ cells isolated from TA2 mouse breast cancer formed more VM channels *in vivo*.

Conclusions: CSCs line VM channels directly. Additionally, CSCs provide more VM-related molecules to synergize VM formation. The signaling pathways that control CSC differentiation may also be potential treatment targets for TNBC.

KEYWORDS   Vasculogenic mimicry; triple-negative breast cancer; cancer stem-like cells; ALDH1; CD133

Introduction

Tumor angiogenesis is an important condition for the growth and evolution of tumors[1]. Tumor angiogenesis involves host blood vessel proliferation and the formation of new blood vessels[1]. Angiogenesis in the bone marrow involves endothelial progenitor cells that are recruited into tumors for colonization and differentiation to form vasculature[2]. Vasculogenic mimicry (VM) involves tumor cells that mimic endothelial cells through deformation and extracellular matrix (ECM) interaction, which surround the lumen and create endothelium-dependent vascular connectivity, becoming functional tumor blood vessels[2-4].

At present, VM in melanoma, hepatocellular carcinoma, ovarian carcinoma, glioma, lung cancer, and more than 10 types of malignant tumors has been identified[5-9]. The presence of VM tumors was associated with a higher degree of malignancy, concerning cell atypia, mitotic figures, invasion, metastasis, and prognosis[1]. The presence of VM tumors increases the risk of hematogenous metastasis and poor survival prognosis[1]. In addition, the structure of VM is composed of tumor cells. Traditional anti-angiogenic drugs targeting endothelial cells are not effective in VM and even promote tumor invasion and metastasis[10-12]. Therefore, finding an effective therapeutic target is the key to improving the prognosis of patients with VM tumors.

The formation of VM is the focus of VM research, such as the ability of VM tumor cells to adopt the pluripotent phenotype of embryonic cells[13,14]. Cancer stem-like cell (CSC) marker expression associated with VM[3] in human malignant tumors suggest that CSCs may participate in the formation of VM. However, there is no direct evidence that

300

Sun et al. Cancer stem-like cells increases VM in TNBC

tumor stem cells are directly involved in the regulation of VM formation.

Previously, VM has been found in human breast cancers, and VM is associated with different breast cancer molecular types[10,15]. There is increased VM in triple-negative breast cancer (TNBC) compared to non-TNBC[10]. The molecular characteristics of TNBC are enriched with cancer stem-like cells[16,17]. In this study, immunohistochemical staining (IHC), multiple fluorescent staining, confocal laser microscopy, and 3D image reconstruction were performed to observe the spatial location relationship between tumor stem cells and VM in TNBC.

Materials and methods

Cells and agents

Human breast cancer MCF-7 cells and MDA-MB-231 cells were purchased from the national experimental cell resource sharing service platform (Beijing). TA2 mouse breast cancer cells were provided by the Animal Department of Tianjin Medical University. The primary antibodies used in this study are listed in **Supplementary Table S1**. All secondary antibodies were purchased from Zhongshan Golden Bridge Biotechnology Co., Ltd. MCF-7 cells, MDA-MB-231 cells, and TA2 mouse breast cancer cells were cultured in RPMI-1640 medium with 10% FBS, 4 mM L-glutamine, and 1% penicillin-streptomycin. Matrigel (BD Bioscience) was diluted with RPMI-1640 medium in 3D cell culture.

Patient samples

All human studies were approved by the Tianjin General Hospital Ethics Committee (Approval No. TMULA-201821). All clinical investigations were conducted according to the principles expressed in the Declaration of Helsinki. The participating patients were informed about the aims, methods, and other details of the medical research. Samples were collected from 100 breast cancer patients with detailed pathological and clinical information. All patients underwent surgery and chemotherapy in Tianjin General Hospital from 1997 to 2004. The median age of the patients was 48.0 years (27 to 74 years). All patients had invasive breast cancer, and 45 cases with axillary node metastasis were reported. The follow-up period ranged from the time of the surgery to December 2008.

IHC staining and counting method

IHC was performed on the tissue microarray sections by following a standard protocol. Protein expression was quantified according to the method of Sun et al. For stain intensity, "0" denoted no staining, "1" denoted weakly positive staining, "2" denoted moderate staining, and "3" denoted strong staining. The number of positive cells out of the 100 tumor cells per field was visually evaluated and scored as follows: "0" for < 10% positive cells, "1" for < 25%, "2" for < 50%, and "3" for > 50%. The staining index, or the sum of the stain intensity and the positive cell score, was used to determine the final result for each sample. A sample was defined as positive when the staining index was greater than 1.

Immunohistochemical staining for CD31 and periodic acid schiff (PAS) histochemical double staining

After IHC for CD31, the sections were exposed to 1% sodium periodate for 10 min. They were incubated for 15 min at PAS at 37°C after washing with distilled water for 5 min. After, the sections were counterstained with hematoxylin and observed under a microscope (80i, Nikon).

FACS analysis

The suspended MDA-MB-231, MCF-7, and TA2 cells were fixed in 75% cold ethanol, and 106 cells were incubated with CD133-PE antibody (1:11 dilution, Miltenyi Biotec) solution or isotype control on ice for 15 min before they were washed and resuspended in staining buffer (2% fetal calf serum in PBS). ALDH1+ cells were detected and isolated with the ALDEFLUORTM stem cell isolation kit (STEMCELL Technologies). 1 mL of the suspended tumor cells was added into the test tubes, and 5 μL ALDEFLUORTM DEAB was added into the control tubes. Activated ALDEFLUOR at a 5 μL volume was added into the test tubes, and half of the mixture in the test tubes was then removed into the control tubes. All tubes were incubated at 37°C for 30 min. Approximately 0.5 mL ALDEFLUOR assay buffer was added to resuspend the cells. All cells were analyzed and isolated using FACSAria III (BD Biosciences). Gates were set with isotype controls such that, for each cell, less than 1% of the total cell population was false-positive. The labeled cells were then analyzed (10,000 events), and the data were saved as FACS.

Serum-free suspension culture of stem cells

MDA-MB-231 cells in different subtypes were collected to culture in a serum-free suspension culture system. Poly2-

hydroxyethyl methacrylate (10 mg/mL in 100% ethanol) was added into 6-well plates (600 μL/plate). The cells were incubated in 6-well plates coated with polyHEMA in serum-free DMEM/F12 media (0.02 g/mL EGF, 0.02 g/mL bFGF, 2%/mL B27). Sphere formation was observed using an inverted microscope (Ts2, Nikon).

Western blot

CD133, ALDH1, E-cadherin, and VE-cadherin protein expression was assessed by western blot. Briefly, total protein was obtained using a lysis buffer (1% SDS, 10 mM Tris-HCl, pH 7.6, 20 μg/mL aprotinin, 20 μg/mL leupeptin and 1 mM AEBSF). Protein concentration was measured using the Bradford method. Approximately 20 μg of protein was separated on an 8% SDS-PAGE gel and blotted onto a PVDF membrane. After blocking with 5% fat-free milk in TBS-Tween overnight, the membrane was incubated with primary antibodies overnight at 4 °C. After washing with TBS-Tween three times, the membrane was labeled with horseradish peroxidase-conjugated anti-goat or IgG (1:1000) for 1 h at room temperature. The blots were developed with a DAB kit, β-actin was used as an internal control, and the bands for the samples were analyzed using a gel imaging system (Kodak).

Immunofluorescent staining

MDA-MB-231 and MCF-7 cells on Matrigel-coated slides were washed with PBS twice, permeabilized, and fixed in 2% PFA and 0.1% Triton X100 in PBS buffer at 4 °C for 30 min. The slides were then washed three times with PBS and incubated with 10% goat serum in PBS. The cells were then incubated with the primary antibodies at 4 °C overnight, washed three times with PBS for 15 min, and incubated with the secondary antibodies for 2 h at room temperature. The slides were washed with PBS and mounted. All matched samples were photographed using a confocal laser scanning microscope (A1, Nikon).

Animal model

The protocols for the animal experiments were approved by the Tianjin Medical University Ethics Committee. All steps were carefully administered to protect the welfare of the animals and prevent their suffering. Nude mice were purchased from Beijing HFK Bioscience Company. Approximately 5×10^6 MDA-MB-231 and MCF-7 tumor cells were subcutaneously injected into the back of six-week-old female mice ($n = 10$/group). Tumors were measured

every 2 d using a standard formula (length × width 2 × 0.52). The nude mice were sacrificed when the MDA-MB-231 and MCF-7 tumor size was close to 0.5 cm³. Fluorescein (494/521)-labeled 2,000,000 MW dextran (D-7137, Molecular Probes™) was injected i.v. 60 min before the mice were sacrificed. Tumors were harvested and fixed in 4% paraformaldehyde for 48 h. The Tientsin Albino 2 (TA2) mice were provided by Animal Center of Tianjin Medical University. Approximately 4×10^5 ALDH1+ and CD133+ TA2 breast cancer cells were subcutaneously injected into the groin of six-week-old female TA2 mice ($n = 10$/group, respectively). The TA2 breast cancer-bearing mice were sacrificed when the tumor size reached up to 1 cm³. Tumors were harvested and fixed in 4% formalin for 24 h. Tumors were embedded in paraffin, and 5 μm-thick sections were prepared.

Whole mount staining

Whole mount staining was performed as described. Briefly, fixed tumors were cut into small pieces (100 - 200 μm), digested with proteinase K (20 μg/mL) for 5 min, and subsequently treated with 100% methanol for 30 min at room temperature. Nonspecific binding sites were blocked overnight at 4°C with a blocking buffer (3% skim milk in PBS containing 0.3% Triton X-100, PBST). Tissue sections were incubated overnight at 4°C with a rat endomucin antibody (1:100 dilution in blocking buffer; 11-5851-80, eBioscience), a rabbit CD133 antibody (1:50 dilution in blocking buffer, Biorbyt), and a rabbit ALDH1 antibody (1:100 dilution in blocking buffer, LSBio). Sections were rigorously washed with PBST four times. Tumor tissues were further blocked using the blocking buffer for an additional 2 h before incubation with the secondary antibody. An Alexa Fluor 680-labeled goat anti-rabbit secondary antibody (1:200, Invitrogen) and a Texas red-labeled goat anti-rat secondary antibody (1:200, Invitrogen) were incubated with tissues at room temperature for 2 h, followed by washing with PBST twice. Stained tissue sections were mounted with a Vectashield mounting medium (ZLI.9557, Zhongshan) and were analyzed by confocal microscopy (Nikon A1 Confocal microscope, Nikon). Positive signal density was quantified using four to six random fields at 10× or 20×, from four to five tumors per group.

Statistics

SPSS version 11.0 (Chicago, Illinois, USA) was used to evaluate the data in this study. The χ^2 test was performed to

302

Sun et al. Cancer stem-like cells increases VM in TNBC

assess the pathological and clinical characteristics of the TNBC and non-TNBC groups. The survival of the two groups was analyzed through a Kaplan-Meier analysis. The relationships between CSC markers, TNBC-type, VM, and VM-related proteins were analyzed by correlation analysis. The two-tailed Student's t test was performed to compare the difference of the two groups in the CSC population, protein expression, VM-like channel counting, fluorescence intensity, and tumor weight. The significance level was set at $P < 0.05$.

Results

Clinical significance of VM and cancer stem-like cells in human breast cancer

In the immunohistochemistry for ER, PR, and HER2 expression, a sample was defined as positive when the staining index was over 1. Among the 100 breast cancer cases in this study, 27 were classified as TNBC and the remaining were non-TNBC. **Figure 1** shows the morphological characteristics. **Supplementary Table 1** shows the difference of VM and CSC marker expression of the TNBC and non-TNBC cases. PAS/CD31 double staining indicated that there was 66.7% with VM in the TNBC group, which was more than the 15.1% in the non-TNBC group ($\chi^2 = 5.270$, $P = 0.020$). Approximately 40.7% of the patients were positive for ALDH1 in the TNBC group, whereas 17.8% of the patients in the non-TNBC group were positive for ALDH1 ($\chi^2 = 6.381$, $P = 0.012$). There were 37.1% of the TNBC cases expressing CD133, while 21.9% expressed CD133 in the non-TNBC group ($\chi^2 = 3.459$, $P = 0.043$). At diagnosis, 33.3% and 19.2% of the TNBC and non-TNBC groups were CD44-positive and CD24-negative ($\chi^2 = 2.652$, $P = 0.090$), respectively.

At the end of the follow-up on December 2008, a total of 71 patients survived. The mean survival of all patients was 86.2 ± 5.6 months. The Kaplan–Meier analysis indicated that the prognosis of the patients with VM was poorer than those without VM (**Figure 2A**, $\chi^2 = 5.907$, $P = 0.015$). The survival of breast cancer patients with more CSCs was poorer than that of patients with fewer CSCs (**Figure 2B**-**2D**).

The relationship between VM and cancer stem-like cells in human breast cancer

Correlation analysis was used to detect the relationship between VM, TNBC type, and CSC marker expression in breast cancer. The results showed that VM was positively correlated with CSC markers ALDH1 and CD44/CD24 (**Table1**). ALDH1 was positively correlated with TNBC type,

VM, and VM-related proteins. CD44+/CD24- breast tumors were positively correlated with TNBC type, VM and HIF-1α.

The difference of ALDH1 and CD133 expression in TNBC MDA-MB-231 and non-TNBC MCF-7 cells

To investigate the difference of CSC marker expression in human breast cancer, TNBC MDA-MB-231 and non-TNBC MCF-7 cells were utilized to assess marker expression and VM formation *in vitro*. FACS indicated that there were more ALDH1+ and CD133+ populations in the TNBC MDA-MB-231 cells than in the MCF-7 cells (**Figure 3A**-**3C**). MDA-MB-231 cells expressed more ALDH1, CD133, and VM-related molecular VE-cadherin (**Figure 3D** and **3E**). MDA-MB-231 cells were more likely to form VM-like channels on Matrigel than MCF-7 cells, and the cells lining VM-like channels were positive for CD133 and ALDH1 (**Figure 3F** and **3G**).

Human cancer stem-like cells promote VM formation in human TNBC

To investigate the influence of CSCs on VM formation, ALDH1+ MDA-MB-231 cells, ALDH1- MDA-MB-231 cells, CD133+ MDA-MB-231 cells, and CD133- MDA-MB-231 cells were isolated to detect their ability to form VM. The ALDH1+ and CD133+ MDA-MB-231 cells formed stem-like cell spheres, while the ALDH1-negative or CD133-negative cells failed to form stem-like cell spheres (**Figure 4A** and **Supplementary Figure S1A**). Western blot showed that the ALDH1+ and CD133+ MDA-MB-231 cells expressed more VE-cadherin than the ALDH1-negative and CD133-negative MDA-MB-231 cells, and less E-cadherin was expressed in these cells (**Figure 4B** and **Supplementary Figure S1B**). Three-dimensional cell culture indicated that the ALDH1+ and CD133+ MDA-MB-231 cells formed VM-like channels; however, the ALDH1-negative and CD133-negative MDA-MB-231 cells lost the ability to form VM channels (**Figure 4C**, **4D** and **Supplementary Figure S1C**, **S1D**). The ALDH1+ and CD133+ MDA-MB-231 cells were more invasive and showed more migration ability than the controls (**Figure 4** and **Supplementary Figure S1**).

Spatial relationship between the expression of stem cell markers and vasculogenic mimicry in breast cancer

In this study, fluorescein-labeled dextran was injected into the peripheral circulation of breast cancer-bearing mice via
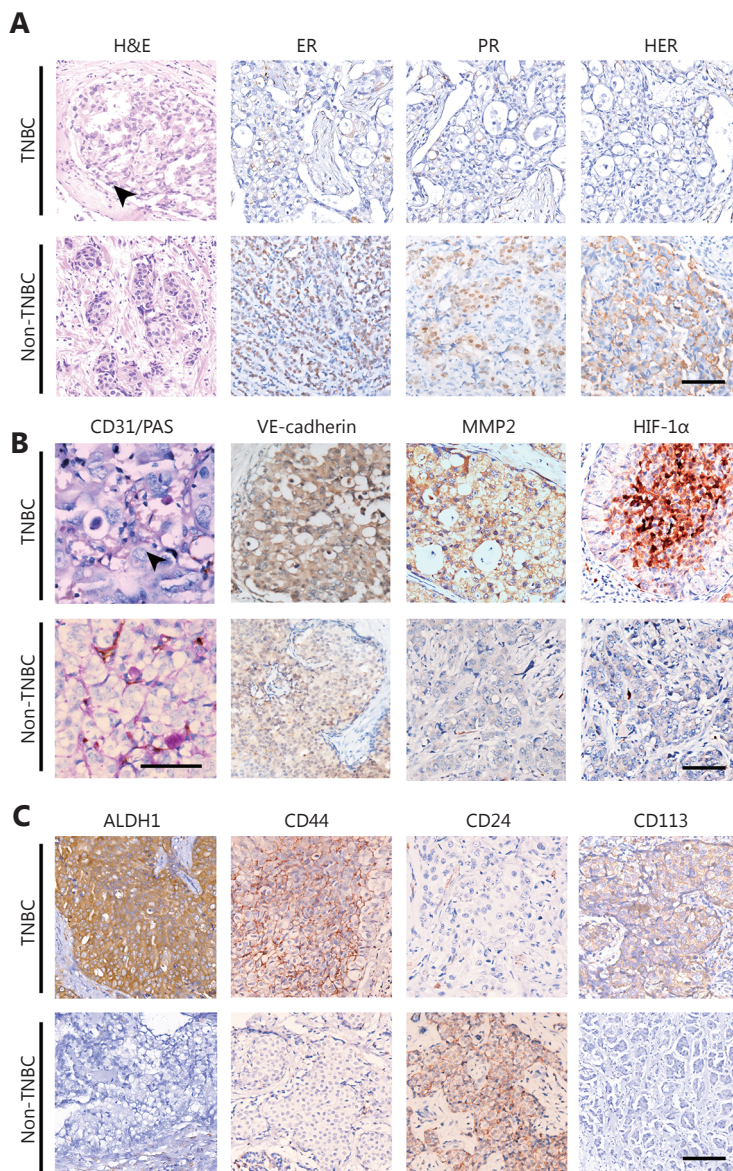
Figure 1 The morphological characteristics of human TNBC and non-TNBC. (A) H&E staining and IHC for ER, PR, and HER2 of human TNBC and non-TNBC. Tumor nests consist of poorly differentiated small tumor cells in TNBC, and necrosis is located in the center of a tumor nest (indicated by a black arrow). A number of tumor cells are undergoing mitosis. (B) Double staining for CD31 and PAS and IHC for VE-cadherin, MMP2, and HIF-1α of human TNBC and non-TNBC. CD31/PAS double staining shows that TNBC has more VM channels compared with non-TNBC. The arrow indicates a VM channel that is formed by a PAS-positive matrix and tumor cells in TNBC. (C) IHC for ALDH1, CD44, CD24, and CD133 of human TNBC and non-TNBC. The scale bar = 100 μm.

tail vein, which marked the blood flow. Then, whole mount staining was used to indicate endothelial cells labeled with red, breast cancer stem cells labeled with blue, and dextran labeled with green. The 3D reconstructed images indicated that the irregular blood flow without endothelium was due to VM channels that were connected to endothelium-dependent vessels. There were more VM vessels and CD133 or ALDH1-positive tumor cells in the MDA-MB-231 tumors than in the MCF-7 tumors (**Figure 5A-5D**). A 3D reconstructed image showed that the CSCs were closer to VM vessels than endothelium-dependent vessels (EDV) (**Figure 5A-5D**).

Cancer stem-like cells promote VM formation in TNBC-bearing mice

TA2 breast cancer was derived from spontaneous breast

Table 1 The correlation of cancer stem-like cells proteins, VM, and VM-associated proteins

		TNBC	VM	ALDH1	CD44/CD24	CD133	VE-Cadherin	MMP2	HIF-1α
TNBC	r	1	0.332**	0.371**	0.164*	0.022	0.112	0.212**	0.264**
	P		0.000	0.000	0.021	0.857	0.089	0.005	0.000
VM	r		1	0.200**	0.206**	0.105	0.200**	0.114	0.147*
	P			0.005	0.003	0.372	0.003	0.133	0.042
ALDH1	r			1	0.082	-0.107	0.250**	0.211**	0.194**
	P				0.251	0.385	0.001	0.005	0.010
CD44/CD24	r				1	0.225	0.020	0.120	0.178*
	P					0.065	0.789	0.113	0.018
CD133	r					1	0.107	0.080	0.106
	P						0.385	0.567	0.445
VE-Cadherin	r						1	0.199*	0.214*
	P							0.011	0.029
MMP2	r							1	0.692**
	P								0.000
HIF-1α	r								1
	P								

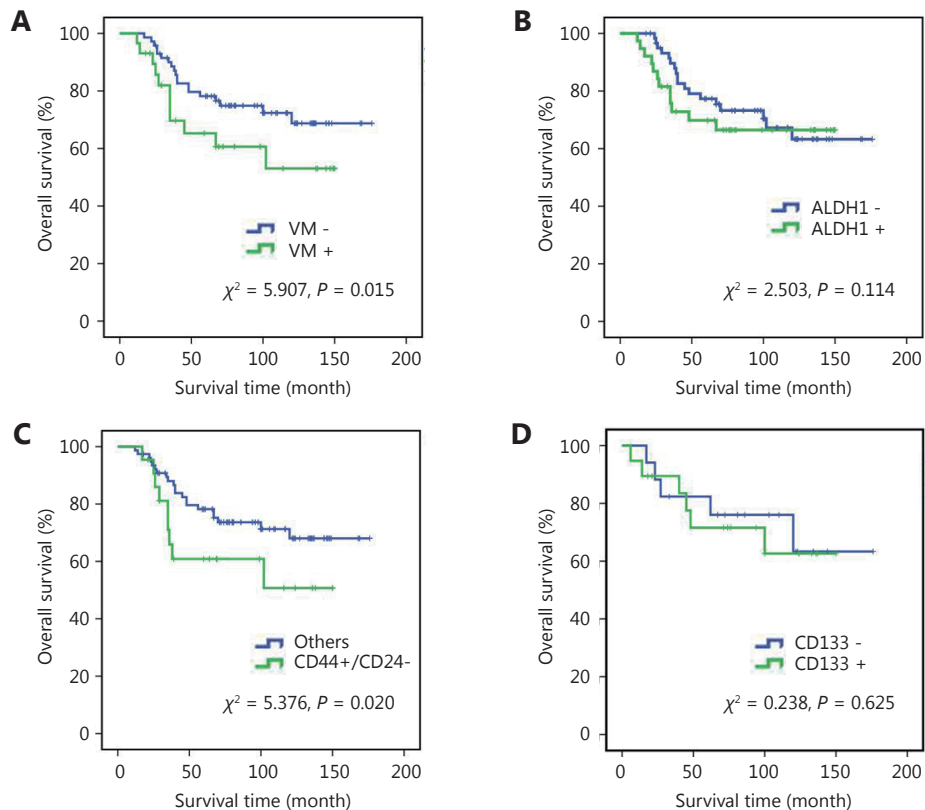* means $P < 0.05$, ** means $P < 0.01$, *** means $P < 0.001$.

Figure 2 Kaplan-Meier survival analysis of human breast cancer. (A) Overall survival of breast cancer with VM and breast cancer without VM. (B) Overall survival of ALDH1+ and ALDH1- breast cancer. (C) Overall survival of CD44+/CD24- and the other breast cancers. (D) Overall survival of CD133+ and CD133- breast cancer.
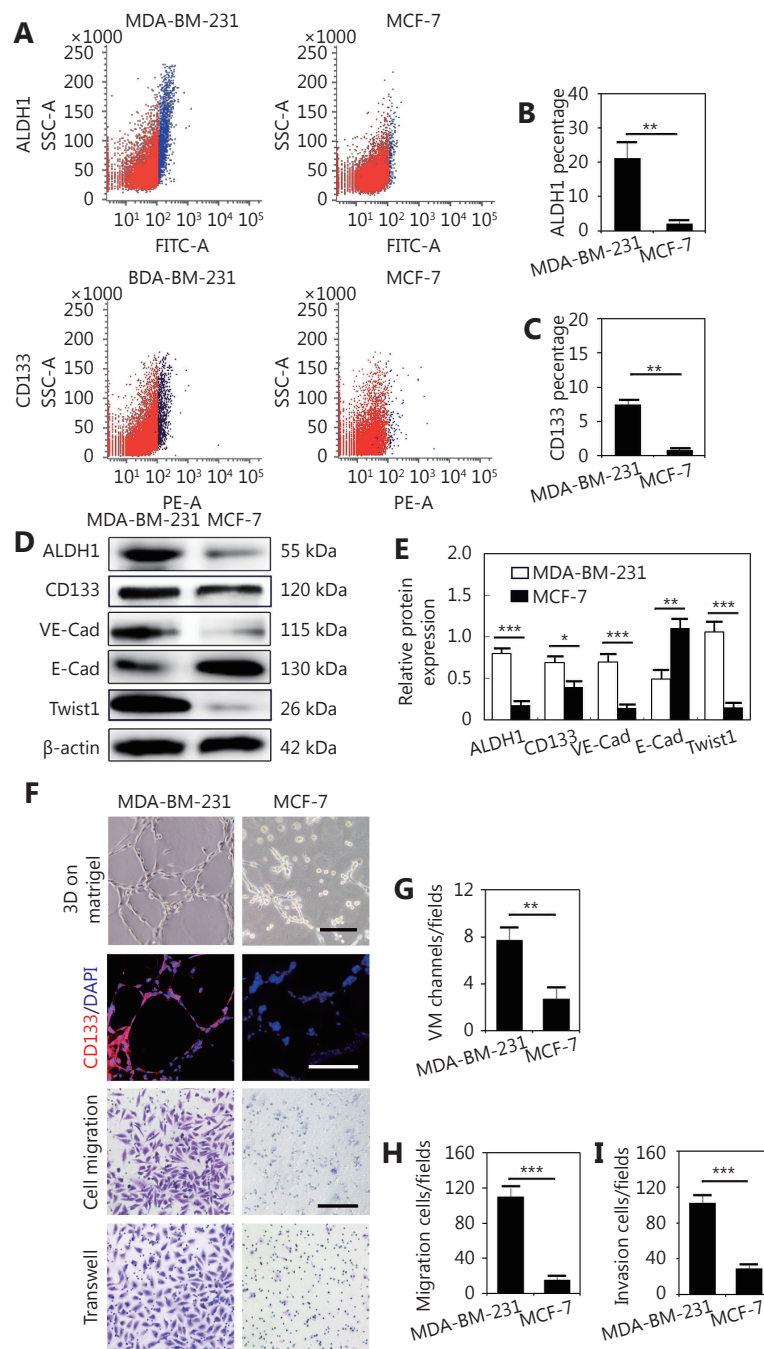
Figure 3 The difference of ALDH1 and CD133 expression in MDA-MB-231 and MCF-7 cells. (A) Representative FACS analyses of the ALDH1+ and CD133+ populations of MDA-MB-231 and MCF-7 cells. (B) Quantification of the ALDH1+ population in MDA-MB-231 and MCF-7 cells. (C) Quantification of the CD133+ population in MDA-MB-231 and MCF-7 cells. (D) Western blot showed the expression of ALDH1, CD133, VE-cadherin, E-cadherin, and Twist1 in MDA-MB-231 and MCF-7 cells. (E) Quantification of the expression of ALDH1, CD133, VE-cadherin, E-cadherin, and Twist1 in MDA-MB-231 and MCF-7 cells. (F) Matrigel cell culture shows that MDA-MB-231 cells formed more VM-like channels than MCF-7 cells on Matrigel. CD133 expressed in MDA-MB-231 cells lining VM. Cell migration and cell invasion analysis of MDA-MB-231 and MCF-7 cells. (G) Quantification of VM-like channels in MDA-MB-231 and MCF-7 cells. (H) Cell migration quantification of MDA-MB-231 and MCF-7 cells. (I) Cell invasion quantification of MDA-MB-231 and MCF-7 cells. The scale bar = 100 μm, and the error bar indicates the SD (standard deviation). ** means $P < 0.01$, *** means $P < 0.001$.
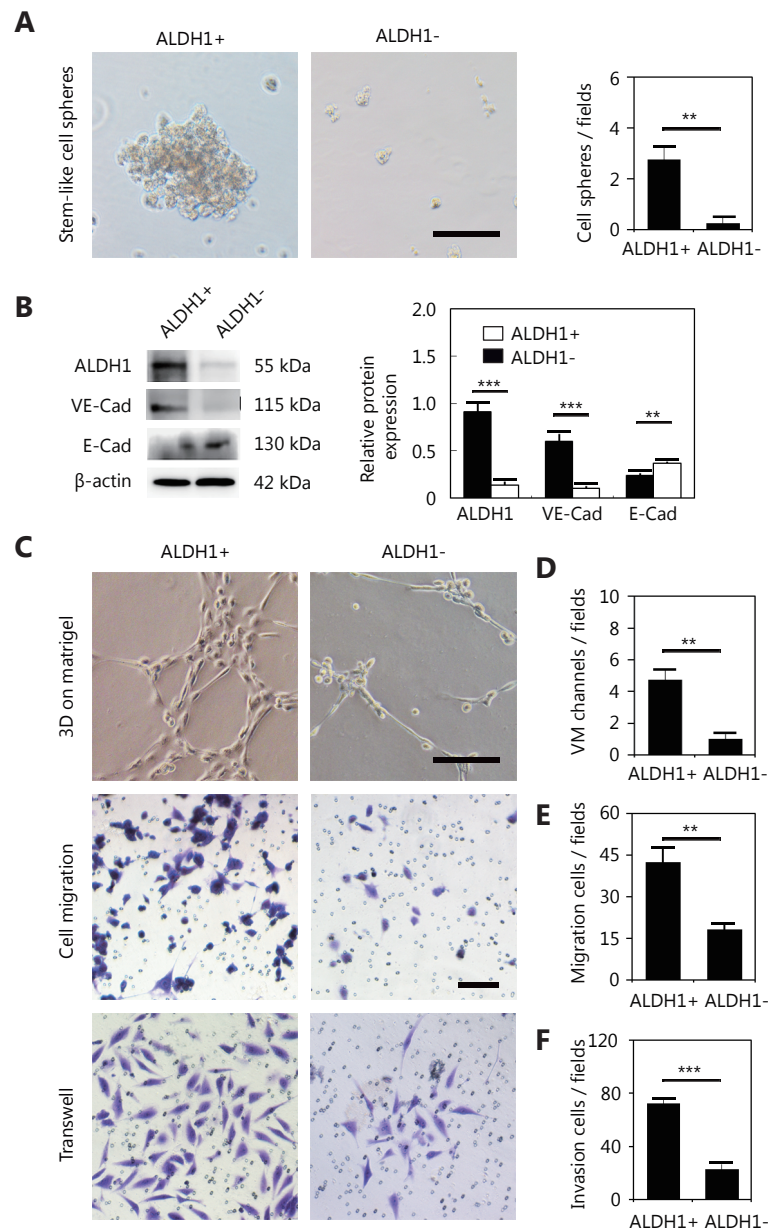
Figure 4 The difference between the ALDH1+ and ALDH1- MDA-MB-231 cells in sphere formation efficiency, VM-associated protein expression, VM-like channel formation, cell migration and cell invasion. (A) Stem-like cell sphere formation of the ALDH1+ and ALDH1- MDA-MB-231 cells. (B) Western blot detection of the expression of ALDH1, VE-cadherin, and E-cadherin in ALDH1+ and ALDH1- MDA-MB-231 cells. Quantification of the Western blot indicates that the ALDH1+ MDA-MB-231 cells expressed more ALDH1 and VE-cadherin than the ALDH1- MDA-MB-231 cells. (C) VM-like channel formation, cell migration and cell invasion of the ALDH1+ and ALDH1- MDA-MB-231 cells. (D) Quantification of VM-like channel formation of the ALDH1+ and ALDH1- MDA-MB-231 cells. (E) Quantification of cell migration of the ALDH1+ and ALDH1- MDA-MB-231 cells. (F) Quantification of cell invasion of the ALDH1+ and ALDH1- MDA-MB-231 cells. The scale bar = 100 μm, and the error bar indicates the SD (standard deviation). ** means $P < 0.01$, *** means $P < 0.001$.

cancer in TA2 mice. These tumors are triple-negative and easily develop metastatic sites in the lungs, liver, and spleen (**Supplementary Figure S2A-S2G**). The tumors expressed a high level of ALDH1 and CD133 (**Supplementary Figure**

S3). To validate the relationship between CSCs and VM in a TNBC animal model, CSCs in TA2 breast cancer cells were isolated and engrafted into mice to detect VM formation and VM-related protein expression. The ratio of tumor formation
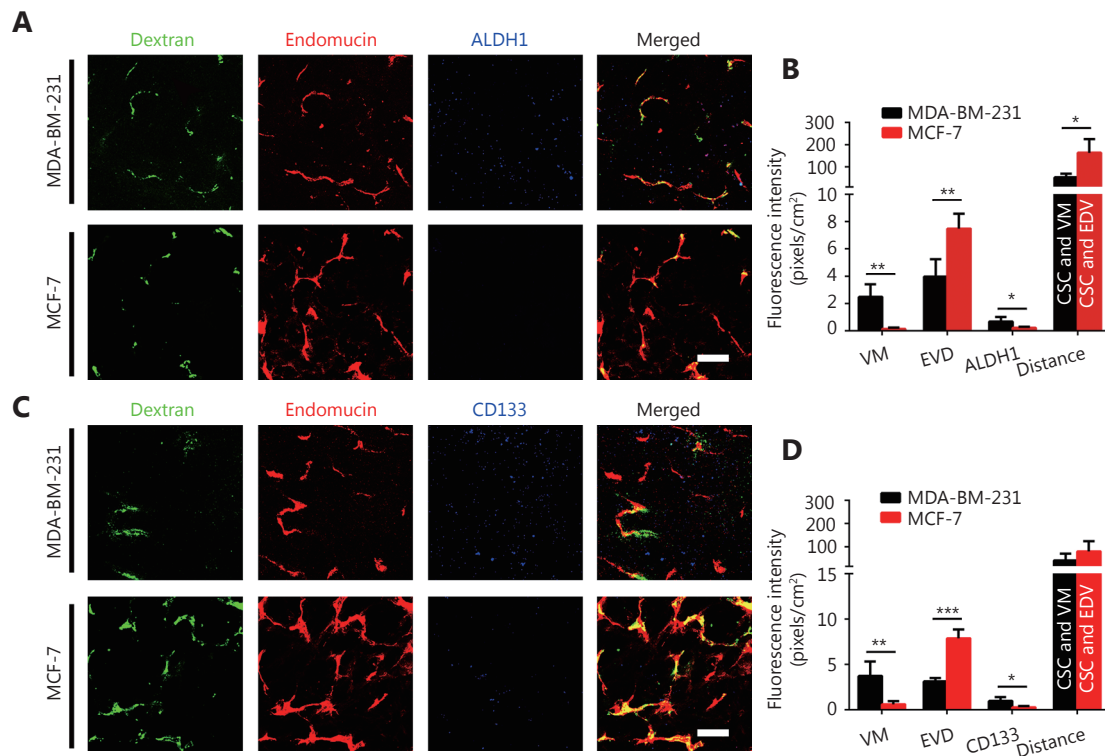
Figure 5 The spatial relationship between breast cancer stem-like cells and tumor microcirculation. (A) 3D image of dextran, EVD and ALDH1+ tumor cells. Laser confocal microscopy indicates that the irregular blood flow of uncoated endothelium is VM channels. (B) Quantification of VM, EVD, and ALDH1+ tumor cells in the MDA-MB-231 and the MCF-7 tumors and distance from ALDH1-positive tumor cells to blood vessels. (C) 3D image of dextran, EVD and CD133+ tumor cells. (D) Quantification of VM, EVD, and CD133+ tumor cells in the MDA-MB-231 and the MCF-7 tumors, and distance from CD133+ tumor cells to blood vessels. The scale bar = 100 μm, and the error bar indicates the standard deviation (SD). * means $P < 0.05$, ** means $P < 0.01$, *** means $P < 0.001$.

and the tumor size in the ALDH1+ tumor cells were higher than those in the ALDH1- tumor cells (**Figure 6A** and **6C**). Similar results were found in the CD133+ and CD133- tumor cells (**Figure 6B** and **6C**). There were more VM channels in the ALDH1+ tumors than the ALDH- tumors, and the CD133+ tumors had more VM channels than the CD133- tumors (**Figure 6D**). The ALDH1+ tumors and the CD133+ tumors expressed more ALDH1, CD133, VE-cadherin, and Twist1 than those in the ALDH1- tumors and the CD133- tumors (**Figure 6E-6H**).

Discussion

VM is lined by tumor cells, and the molecular mechanisms of VM formation are independent from the mechanisms regulating EDV[2,18]. The traditional anti-angiogenic agents target the molecular signaling pathway that regulates endothelial cells[4,19]. Recently, sunitinib, an inhibitor of VEGF receptor tyrosine kinase activity, accelerated the recurrence

and visceral metastasis of VM-positive TNBC in an animal model[10]. Hypoxia induced by inhibition of EDV vessels caused VM formation, which provided the blood supply instead of EDV vessels. VM is partly responsible for the resistance of anti-angiogenic treatment to TNBC[10]. Inhibition of VM will require understanding of the molecular mechanism of VM.

VM tissues are PAS+/CD31-/CD34- and do not respond to Ulex europaeus agglutinin-1 by immunohistochemistry[20-21]. Cells lining VM channels maintain some characteristics of the malignant tumor but also have some endothelial cell functions and phenotypes[20,22]. VM-initiating cells are of particular interest to investigators. The formation of VM in malignant tumors is similar to vasculogenesis in embryonic development[23-25]. Folberg et al. and Seftor et al. found that melanoma cell lines with VM expressed not only melanoma cell-specific genes but also multiple genes that regulate cell plasticity in embryogenesis[13,24]. CSCs were associated with VM formation in malignant tumors. CSC markers CD133

308

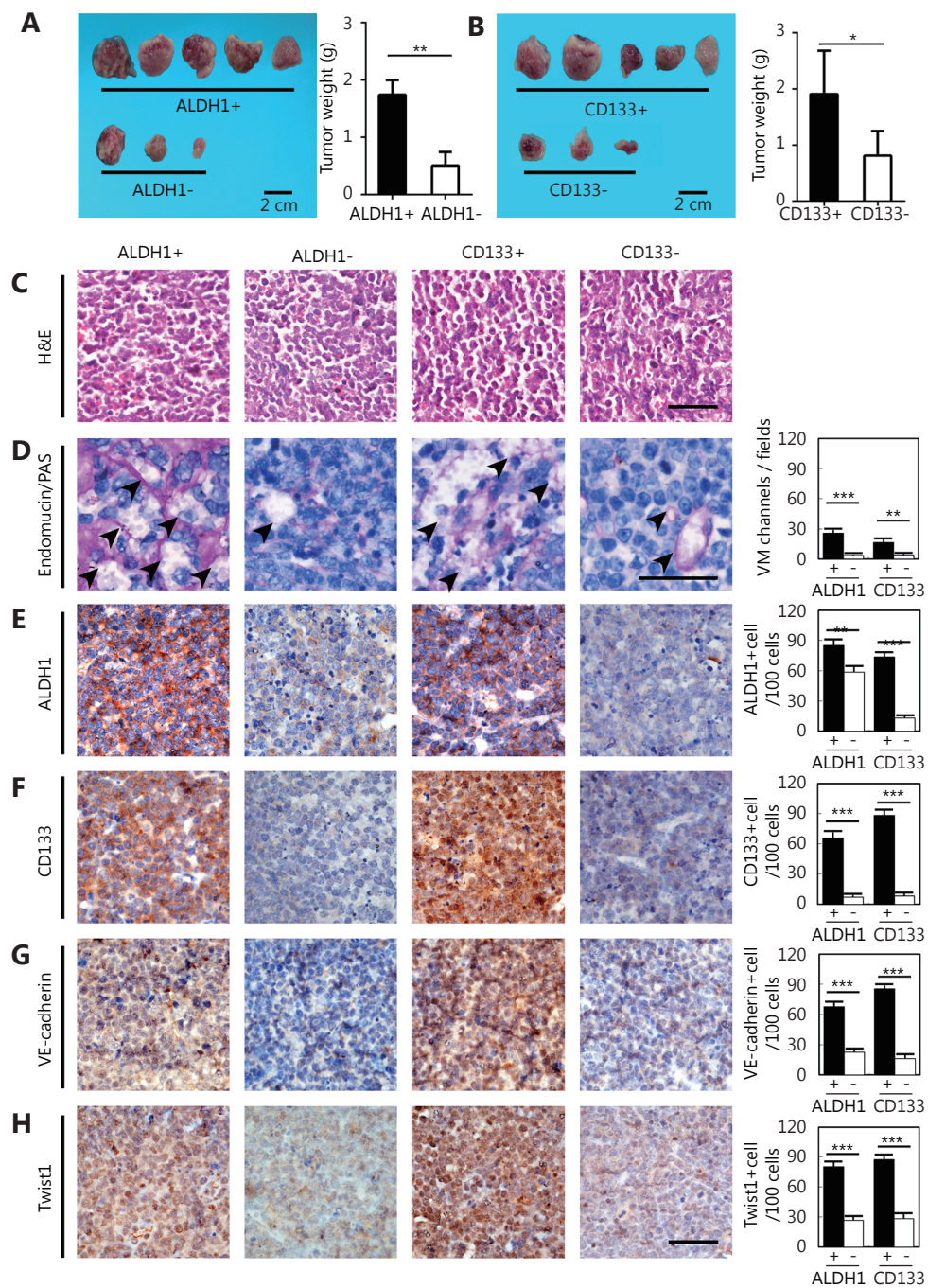Sun et al. Cancer stem-like cells increases VM in TNBC

Figure 6 Effects of ALDH1+ and CD133+ tumor cells on TA2 breast tumor growth and VM-associated molecule expression. (A) Tumor size and tumor weight of ALDH1+ and CD133+ TA2 breast tumors. (B) H&E staining of ALDH1+ and CD133+ TA2 breast tumors. (C) Double staining for endomucin and PAS of ALDH1+ and CD133+ TA2 breast tumors. Quantification of VM number indicates that there are more VM channels in the ALDH1+ tumors than the ALDH- tumors, and the CD133+ tumors have more VM channels than the CD133- tumors. (E) IHC staining for ALDH1 in ALDH1+ and CD133+ TA2 breast tumors and quantification of ALDH1+ cells in different groups. (F) IHC staining for CD133 in ALDH1+ and CD133+ TA2 breast tumors and quantification of CD133+ cells in different groups. (G) IHC staining for VE-cadherin in ALDH1+ and CD133+ TA2 breast tumors and quantification of VE-cadherin cells in different groups. (H) IHC staining for Twist1 in ALDH1+ and CD133+ TA2 breast tumors and quantification of Twist1-positive cells in different groups. The scale bar = 100 μm, and the error bar indicates the standard deviation (SD). * means $P < 0.05$, ** means $P < 0.01$, *** means $P < 0.001$.

and CD44 were significantly correlated with VM existence in human renal cell carcinoma[26]. Hepatocellular carcinoma cells lining VM channels expressed SOX2 and OCT4[27]. A neural precursor marker, nestin, and multiple stem cell markers, including CD133, Oct4, Nanog, and Notch1, were expressed in U87 glioma xenografts and human non-small lung carcinomas with VM[28].

In this study, CSC markers in breast cancer CD133, ALDH1, and CD44+/CD24- were positively correlated with VM and molecules involved in VM formation[29]. CSC markers were also related to TNBC subtype[30-32]. There were more tumors with VM in the TNBC group than in the non-TNBC group. TNBC cells express stem cell-specific markers and markers specific to mesenchymal stem cells[6,33]. Moreover, human TNBC cells MDA-MB-231 were enriched with ALDH1 and CD133 and had a higher capability to form VM than that of non-TNBC MCF-7 cells. Therefore, the results in this study confirmed that CSCs participated in VM formation.

Furthermore, ALDH1+ and CD133+ CSCs isolated from MDA-MB-231 and mouse TNBC cells formed VM channels *in vitro* and *in vivo*, while ALDH1-negative or CD133-negative breast cancer cells failed to form VM channels. MDA-MB-231 cells lining VM channels on Matrigel expressed CD133. Three-dimensional reconstructed images showed the spatial relationship between VM and CSCs. The CSCs were closer to VM vessels than to EDV vessels. These results directly indicated that tumor cells lining VM channels were derived from CSCs. Previous studies focused on the differentiation of CSCs into endothelium-like cells *in vitro*. In this study, three-dimensional reconstructed images showed the spatial relationship between VM and CSCs in an animal model. The results showed that the CSCs were closer to VM vessels than to EDV vessels. These results directly indicated that tumor cells lining VM channels were derived from CSCs.

CSCs can differentiate into multiple cell types[34,35]. Tumor generation and metastasis are based on CSC self-renewal and differentiation[34-36]. Many tumor endothelial cells have neoplastic origins[37-40]. Glioblastoma stem-like cells were successfully induced to differentiate into functional endothelial cells[38]. Glioblastoma and endothelial cells carry the same genomic alterations as tumor cells[37]. Tumors resistant to existing treatments have also been attributed to CSCs in malignant tumors[41]. CSCs are the source of tumor relapse and metastasis after treatment[41]. The differentiation and behavior of CSCs were the results of the responses of the tumor cells to the tumor microenvironment. For example, hypoxia caused by anti-angiogenic agents can contribute to CSC survival and metastatic potential[42-43]. Sunitinib, an anti-

angiogenic drug targeting the endothelium, caused more CD133+ subpopulation and VM formation in human TNBC grafts[10]. Hence, signaling pathways in CSCs and VM might be the target of anti-angiogenesis in malignant tumors.

There is more evidence that epithelial-mesenchymal transition (EMT) is an important promoter for VM formation in many malignant tumors[2,44]. The process of epithelial tumors transitioning to VM cells with mesenchymal features is similar to EMT in embryogenesis[2,20]. Many transcriptional factors involved in EMT, such as Twist1, Slug, bone morphogenetic protein 4 (BMP4), and Dickkopf-1 (DKK1), can induce VM formation[6,27,45]. Recent evidence revealed that EMT and CSCs have synergistic effects in VM promotion. Upregulation of high mobility group AT-hook 2 (HMGA2) resulted in gastric cancer cell VM and sphere formation[46]. The CSC markers CD44, ALDH1, Sox2, and Oct4 are also expressed at an increased level[46]. DKK1 also induced VM and the development of a CSC phenotype in non-small lung carcinoma[6]. Twist1 expression is related to TNBC tumors. There was a higher level of Twist1 in MDA-MB-231 cells than in the MCF-710 cells. ADLH1+ and CD133+ TA2 breast cancer grafts expressed a high level of Twist1 and formed more VM channels. Inhibition of Twist1 disrupted the VM and reduced the CD133+ population in MDA-MB-231. Alternatively, upregulation of EMT-regulating factors can also be induced by stem cell molecules. IMP3 and Sox2 induced Snail and Slug to promote EMT and metastasis in breast cancer[47]. Here, we showed that CD133+ and ALDH1+ MDA-MB-231 cells expressed more Twist1 and VM-related VE-cadherin, which accelerates VM formation and tumor metastasis. This confirmed that there is some interaction between CSC differentiation and the EMT signaling pathway.

The Notch pathway is central to controlling cell fate both during angiogenesis and in CSCs from several tumors[14,48]. Notch4 is also involved in VM formation in melanoma and promoted CSC marker expression[48-49]. Notch4 regulates the expression of Nodal, a member of the TGF-β superfamily, by inducing the activity of an RBPJ-dependent pathway in an aggressive melanoma cell line[49]. The induction of Notch4 on Nodal is partly responsible for VM formation in melanoma. There are several Notch inhibitors, such as MK-0752 and N-[N-(3,5-difluorophenacetyl-L-alanyl)]-S-phenylglycine-t-butyl ester, which can reverse Notch4 effects in melanoma and pancreatic ductal adenocarcinoma cells[50,51]. Hence, they may be candidates for treatment of malignant tumors with VM.

In conclusion, CSCs lined VM channels directly. Additionally, CSCs provide more VM-related molecules to

310

Sun et al. Cancer stem-like cells increases VM in TNBC

synergize VM formation. The signaling pathways that control CSC differentiation may also be potential therapeutic targets for TNBC.

Acknowledgments

Conflict of interest statement

No potential conflicts of interests are disclosed.

References

1. Watnick RS, Cheng YN, Rangarajan A, Ince TA, Weinberg RA. Ras modulates Myc activity to repress thrombospondin-1 expression and increase tumor angiogenesis. Cancer Cell. 2003; 3: 219-31.

2. Sun BC, Zhang DF, Zhao N, Zhao XL. Epithelial-to-endothelial transition and cancer stem cells: two cornerstones of vasculogenic mimicry in malignant tumors. Oncotarget. 2017; 8: 30502-10.

3. Jones EA, le Noble F, Eichmann A. What determines blood vessel structure? Genetic prespecification vs. Hemodynamics Physiology (Bethesda). 2006; 21: 388-95.

4. Seftor RE, Hess AR, Seftor EA, Kirschmann DA, Hardy KM, Margaryan NV, et al. Tumor cell vasculogenic mimicry: from controversy to therapeutic promise. Am J Pathol. 2012; 181: 1115-25.

5. Seftor EA, Seftor REB, Weldon DS, Kirsammer GT, Margaryan NV, Gilgur A, et al. Melanoma tumor cell heterogeneity: a molecular approach to study subpopulations expressing the embryonic morphogen nodal. Semin Oncol. 2014; 41: 259-66.

6. Yao LL, Zhang DF, Zhao XL, Sun BC, Liu YR, Gu Q, et al. Dickkopf-1-promoted vasculogenic mimicry in non-small cell lung cancer is associated with EMT and development of a cancer stem-like cell phenotype. J Cell Mol Med. 2016; 20: 1673-85.

7. Sun T, Sun BC, Zhao XL, Zhao N, Dong XY, Che N, et al. Promotion of tumor cell metastasis and vasculogenic mimicry by way of transcription coactivation by Bcl-2 and Twist1: a study of hepatocellular carcinoma. Hepatology. 2011; 54: 1690-706.

8. Du J, Sun BC, Zhao XL, Gu Q, Dong XY, Mo J, et al. Hypoxia promotes vasculogenic mimicry formation by inducing epithelial-mesenchymal transition in ovarian carcinoma. Gynecol Oncol. 2014; 133: 575-83.

9. Zhang L, Xu YY, Sun JT, Chen WL, Zhao L, Ma C, et al. M2-like tumor-associated macrophages drive vasculogenic mimicry through amplification of IL-6 expression in glioma cells. Oncotarget. 2017; 8: 819-32.

10. Zhang DF, Sun BC, Zhao XL, Ma YM, Ji R, Gu Q, et al. Twist1 expression induced by sunitinib accelerates tumor cell vasculogenic mimicry by increasing the population of CD133+ cells in triple-negative breast cancer. Mol Cancer. 2014; 13: 207.

11. Sasanelli F, Hocking A, Pulford E, Irani Y, Klebe S. Vasculogenic mimicry *in vitro* in tumour cells derived from metastatic malignant pleural effusions. Pathology. 2017; 49: 537-39.

12. Dunleavey JM, Dudley AC. Vascular mimicry: concepts and implications for anti-angiogenic therapy. Curr Angiogenes. 2012; 1: 133-8.

13. Seftor EA, Meltzer PS, Schatteman GC, Gruman LM, Hess AR, Kirschmann DA, et al. Expression of multiple molecular phenotypes by aggressive melanoma tumor cells: role in vasculogenic mimicry. Crit Rev Oncol Hematol. 2002; 44: 17-27.

14. Gu JW, Rizzo P, Pannuti A, Golde T, Osborne B, Miele L. Notch signals in the endothelium and cancer "Stem-like" Cells: opportunities for cancer therapy. Vasc Cell. 2012; 4: 7.

15. Wang Y, Sun HZ, Zhang DF, Fan D, Zhang YH, Dong XY, et al. TP53INP1 inhibits hypoxia-induced vasculogenic mimicry formation via the ROS/snail signalling axis in breast cancer. J Cell Mol Med. 2018; 22: 3475-88.

16. Lehmann BD, Bauer JA, Chen X, Sanders ME, Chakravarthy AB, Shyr Y, et al. Identification of human triple-negative breast cancer subtypes and preclinical models for selection of targeted therapies. J Clin Invest. 2011; 121: 2750-67.

17. de Azambuja E, Cardoso F, Meirsman L, Straehle C, Dolci S, Vantongelen K, et al. The new generation of breast cancer clinical trials: the right drug for the right target. Bull Cancer. 2008; 95: 352-7.

18. Kirschmann DA, Seftor EA, Hardy KM, Seftor REB, Hendrix MJC. Molecular pathways: vasculogenic mimicry in tumor cells: diagnostic and therapeutic implications. Clin Cancer Res. 2012; 18: 2726-32.

19. Kurzrock R, Stewart DJ. Exploring the benefit/risk associated with antiangiogenic agents for the treatment of non-small cell lung cancer patients. Clin Cancer Res. 2017; 23: 1137-48.

20. Hendrix MJC, Seftor EA, Hess AR, Seftor REB. Vasculogenic mimicry and tumour-cell plasticity: lessons from melanoma. Nat Rev Cancer. 2003; 3: 411-21.

21. Maniotis AJ, Folberg R, Hess A, Seftor EA, Gardner LMG, Pe'er J, et al. Vascular channel formation by human melanoma cells *in vivo* and *in vitro*: vasculogenic mimicry. Am J Pathol. 1999; 155: 739-52.

22. Hendrix MJC, Seftor EA, Hess AR, Seftor REB. Molecular plasticity of human melanoma cells. Oncogene. 2003; 22: 3070-5.

23. Mei X, Chen YS, Chen FR, Xi SY, Chen ZP. Glioblastoma stem cell differentiation into endothelial cells evidenced through live-cell imaging. Neuro Oncol. 2017; 19: 1109-18.

24. Folberg R, Arbieva Z, Moses J, Hayee A, Sandal T, Kadkol S, et al. Tumor cell plasticity in uveal melanoma: microenvironment directed dampening of the invasive and metastatic genotype and phenotype accompanies the generation of vasculogenic mimicry patterns. Am J Pathol. 2006; 169: 1376-89.

25. Huang MG, Liu TR, Ma PH, Mitteer RA Jr, Zhang ZT, Kim HJ, et al. c-Met-mediated endothelial plasticity drives aberrant vascularization and chemoresistance in glioblastoma. J Clin Invest. 2016; 126: 1801-14.

26. Zhang YH, Sun BC, Zhao XL, Liu ZY, Wang XD, Yao X, et al. Clinical significances and prognostic value of cancer stem-like cells markers and vasculogenic mimicry in renal cell carcinoma. J Surg Oncol. 2013; 108: 414-9.

27. Zhao XL, Sun BC, Sun D, Liu TJ, Che N, Gu Q, et al. Slug promotes hepatocellular cancer cell progression by increasing sox2 and nanog expression. Oncol Rep. 2015; 33: 149-56.

28. Francescone R, Scully S, Bentley B, Yan W, Taylor SL, Oh D, et al. Glioblastoma-derived tumor cells induce vasculogenic mimicry through Flk-1 protein activation. J Biol Chem. 2012; 287: 24821-31.

29. Comănescu M, Bussolati G. Cancer stem cells biomarkers in triple negative invasive carcinoma of the breast and associated *in situ* lesions. Rom J Morphol Embryol. 2014; 55: 569-74.

30. Curtis C, Shah SP, Chin SF, Turashvili G, Rueda OM, Dunning MJ, et al. The genomic and transcriptomic architecture of 2, 000 breast tumours reveals novel subgroups. Nature. 2012; 486: 346-52.

31. Tsukabe M, Shimazu K, Morimoto K, Naoi Y, Kagara N, Shimoda M, et al. Clinicopathological analysis of breast ductal carcinoma in situ with ALDH1-positive cancer stem cells. Oncology. 2013; 85: 248-56.

32. Idowu MO, Kmieciak M, Dumur C, Burton RS, Grimes MM, Powers CN, et al. CD44$^+$/CD24$^{-/low}$ cancer stem/progenitor cells are more abundant in triple-negative invasive breast carcinoma phenotype and are associated with poor outcome. Hum Pathol. 2012; 43: 364-73.

33. Chiche A, Moumen M, Romagnoli M, Petit V, Lasla H, Jézéquel P, et al. p53 deficiency induces cancer stem cell pool expansion in a mouse model of triple-negative breast tumors. Oncogene. 2017; 36: 2355-65.

34. Pohl SG, Brook N, Agostino M, Arfuso F, Kumar AP, Dharmarajan A. Wnt signaling in triple-negative breast cancer. Oncogenesis. 2017; 6: e310.

35. Prieto-Vila M, Yan T, Calle AS, Nair N, Hurley L, Kasai T, et al. iPSC-derived cancer stem cells provide a model of tumor vasculature. Am J Cancer Res. 2016; 6: 1906-21.

36. Nwabo Kamdje AH, Kamga PT, Simo RT, Vecchio L, Seke Etet PF, Muller JM, et al. Mesenchymal stromal cells' role in tumor microenvironment: involvement of signaling pathways. Cancer Biol Med. 2017; 14: 129-141.

37. Wang R, Chadalavada K, Wilshire J, Kowalik U, Hovinga KE, Geber A, et al. Glioblastoma stem-like cells give rise to tumour endothelium. Nature. 2010; 468: 829-33.

38. Ricci-Vitiani L, Pallini R, Biffoni M, Todaro M, Invernici G, Cenci T, et al. Tumour vascularization via endothelial differentiation of glioblastoma stem-like cells. Nature. 2010; 468: 824-8.

39. Guelfi S, Duffau H, Bauchet L, Rothhut B, Hugnot JP. Vascular transdifferentiation in the CNS: a focus on neural and glioblastoma stem-like cells. Stem Cells Int. 2016; 2016: 2759403.

40. Bussolati B, Grange C, Sapino A, Camussi G. Endothelial cell differentiation of human breast tumour stem/progenitor cells. J Cell Mol Med. 2009; 13: 309-19.

41. Shima H, Yamada A, Ishikawa T, Endo I. Are breast cancer stem cells the key to resolving clinical issues in breast cancer therapy? Gland Surg. 2017; 6: 82-8.

42. Zhang CZ, Samanta D, Lu HQ, Bullen JW, Zhang HM, Chen I, et al. Hypoxia induces the breast cancer stem cell phenotype by HIF-dependent and ALKBH5-mediated m^{6}A-demethylation of NANOG mRNA. Proc Natl Acad Sci USA. 2016; 113: E2047-56.

43. Conley SJ, Gheordunescu E, Kakarala P, Newman B, Korkaya H, Heath AN, et al. Antiangiogenic agents increase breast cancer stem cells via the generation of tumor hypoxia. Proc Natl Acad Sci USA. 2012; 109: 2784-9.

44. Wang H, Huang B, Li BM, Cao KY, Mo CQ, Jiang SJ, et al. ZEB1-mediated vasculogenic mimicry formation associates with epithelial-mesenchymal transition and cancer stem cell phenotypes in prostate cancer. J Cell Mol Med. 2018; 22: 3768-81.

45. Rothhammer T, Bataille F, Spruss T, Eissner G, Bosserhoff AK. Functional implication of BMP4 expression on angiogenesis in malignant melanoma. Oncogene. 2007; 26: 4158-70.

46. Sun JY, Sun BC, Sun R, Zhu DW, Zhao XL, Zhang YH, et al. HMGA2 promotes vasculogenic mimicry and tumor aggressiveness by upregulating twist1 in gastric carcinoma. Sci Rep. 2017; 7: 2229.

47. Samanta S, Sun H, Goel HL, Pursell B, Chang C, Khan A, et al. IMP3 promotes stem-like properties in triple-negative breast cancer by regulating SLUG. Oncogene. 2016; 35: 1111-21.

48. Nwabo Kamdje AH, Takam Kamga P, Tagne Simo R, Vecchio L, Seke Etet PF, Muller JM, et al. Developmental pathways associated with cancer metastasis: notch, Wnt, and hedgehog. Cancer Biol Med. 2017; 14: 109-20.

49. Hardy KM, Kirschmann DA, Seftor EA, Margaryan NV, Postovit LM, Strizzi L, et al. Regulation of the embryonic morphogen Nodal by Notch4 facilitates manifestation of the aggressive melanoma phenotype. Cancer Res. 2010; 70: 10340-50.

50. Piha-Paul SA, Munster PN, Hollebecque A, Argilés G, Dajani O, Cheng JD, et al. Results of a phase 1 trial combining ridaforolimus and MK-0752 in patients with advanced solid tumours. Eur J Cancer. 2015; 51: 1865-73.

51. Nagamatsu I, Onishi H, Matsushita S, Kubo M, Kai M, Imaizumi A, et al. NOTCH4 is a potential therapeutic target for triple-negative breast cancer. Anticancer Res. 2014; 34: 69-80.

Supplementary materials

Table S1 Information of primary antibodies used in this study

Antibody	Source	NO.	Company	Dilution
ALDH1	Rabbit			
CD133	Rabbit		Miltenyi Biotec GmbH	1:100
CD44	Rabbit	ZA-0537	Zhongshan Golden Bridge	ready-to-use
CD24	Rabbit	NBP1-46390	Novus Bio	1:200
HIF-1α	Rabbit	ZA-0552	Zhongshan Golden Bridge	ready-to-use
MMP2	Rabbit	10373-2-Ap	Luosai	1:100
VE-cadherin	Rat	ab33168	Abcam	1:200
Twist1	Rabbit	sc-15393	Santa cruz	1:200
Endomucin	Rat	11-5851-80	eBioscience	1:400
ER	Mouse	ZM-0104	Zhongshan Golden Bridge	ready-to-use
PR	Rabbit	C-20, sc-539	Zhongshan Golden Bridge	1:100
HER2	Mouse	ZM-0041	Zhongshan Golden Bridgse	ready-to-use
CD31	Mouse	ZM-0044	Zhongshan Golden Bridge	ready-to-use

Table S2   Comparison of pathological and clinical features between triple-negative and non-triple-negative breast cancer cases

Factors	Triple-negative (%)27	Non-triple-negative (%) 73	χ^2	P
Age (years)				
< 40	9 (33.3)	10 (13.7)	4.937	0.026*
≥ 40	18 (66.7)	63 (86.3)		
Tumor size (diameter)				
d < 2 cm	6 (21.7)	20 (27.4)	0.415	0.831
2 ≤ d < 5 cm	19 (70.9)	49 (66.8)		
d ≥ 5	2(7.4)	4 (5.8)		
Grade				
I and II	15 (56.5)	54 (73.9)	2.545	0.111
III	12 (43.5)	19 (26.1)		
Axillary node status				
Negative	17 (63.0)	38(52.1)	0.948	0.333
Positive	10 (37.0)	35 (47.9)		
TNM stage				
I - II	23 (85.2)	63 (86.3)	0.510	0.082
III - IV	4 (14.8)	10 (13.7)		
VM				
Negative	9 (33.3)	62 (84.9)	5.270	0.020*
Positive	18 (66.7)	11 (15.1)		
ALDH1				
Negative	16 (59.3)	60 (82.2)	6.381	0.012**
Positive	11 (40.7)	13 (17.8)		
CD133				
Negative	17 (62.9)	57 (78.1)	3.459	0.043*
Positive	12 (37.1)	16 (21.9)		
CD44+\CD24-				
Negative	18 (66.7)	59 (80.8)	2.652	0.090
Positive	9 (33.3)	14 (19.2)		
VE-cadherin				
Negative	9 (33.3)	35 (48.5)	1.988	0.159
Positive	18 (66.7)	38 (51.5)		

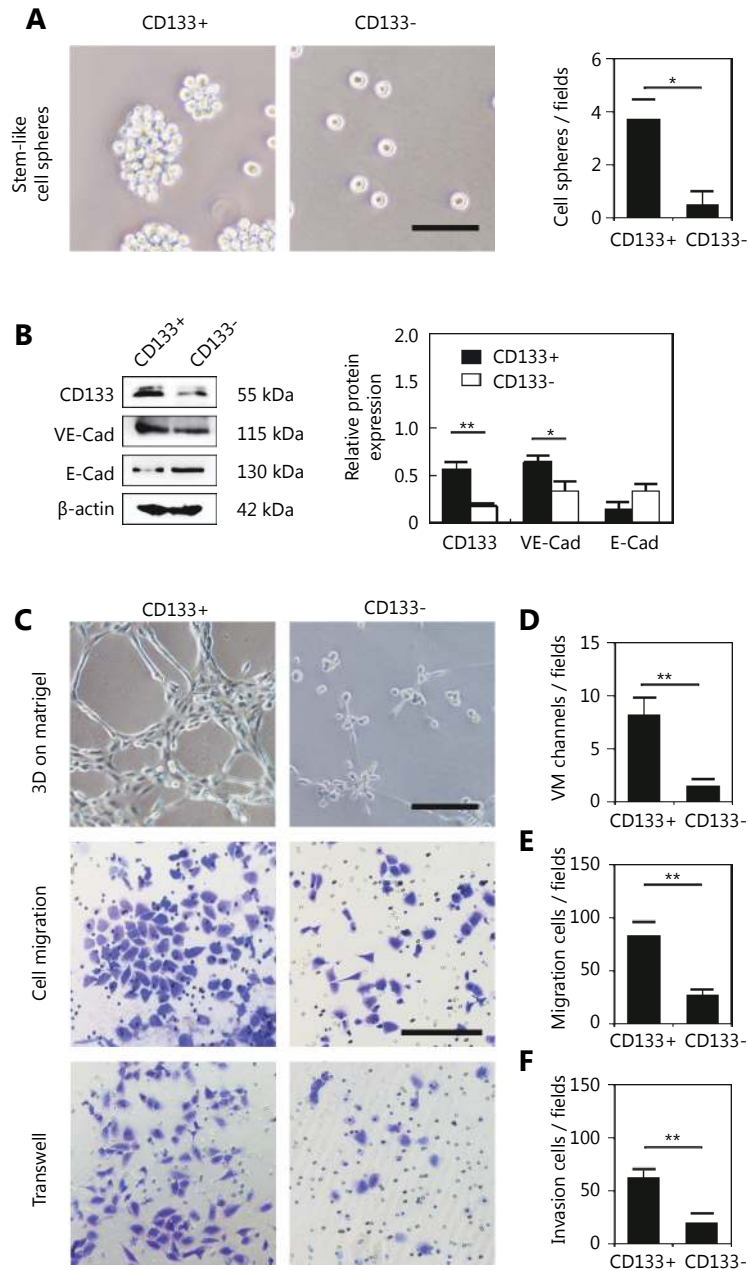$P < 0.05$; ** $P < 0.01$; *** $P < 0.001$

Figure S1 The difference between the CD133+ and CD133- MDA-MB-231 cells in sphere formation efficiency, VM-associated protein expression, VM-like channel formation, cell migration and cell invasion. (A) Stem-like cell sphere formation of the CD133+ and CD133- MDA-MB-231 cells. (B) Western blot detection of the expression of CD133, VE-cadherin, and E-cadherin in CD133+ and CD133- MDA-MB-231 cells. Quantification of the western blots indicates that the CD133+ MDA-MB-231 cells expressed more CD133 and VE-cadherin than the CD133- MDA-MB-231 cells. (C) VM-like channel formation, cell migration and cell invasion of the CD133+ and CD133- MDA-MB-231 cells. (E) Quantification of VM-like channel formation of the CD133+ and CD133- MDA-MB-231 cells. (F) Quantification of cell migration of the CD133+ and CD133- MDA-MB-231 cells. (G) Quantification of cell invasion of the CD133+ and CD133- MDA-MB-231 cells. The scale bar = 100 μm, and the error bar indicates the SD (standard deviation). * means P <0.05, ** means P < 0.01.
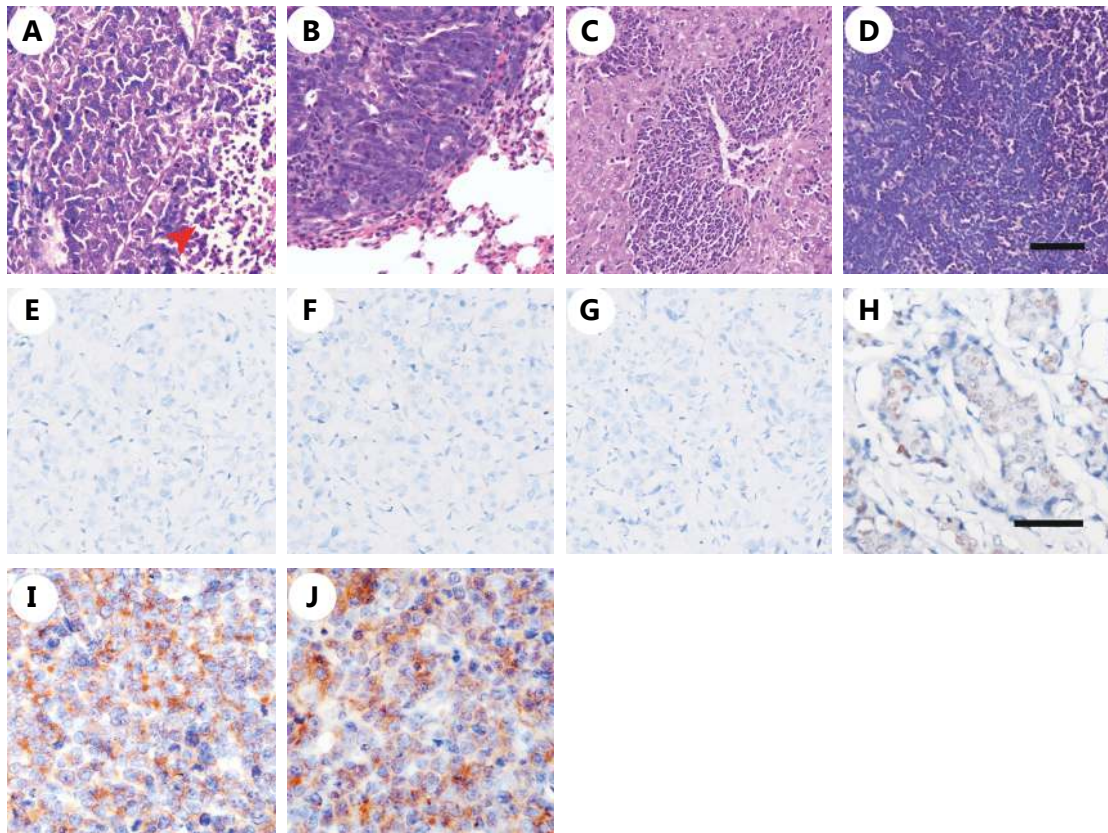
Figure S2 Morphological and molecular characterization of breast cancer in TA2 mice. (A) Breast cancers in TA2 mice are mostly composed of poorly differentiated cells, and they form various tumor nests separated by well-developed stroma. Necrosis (arrow) is frequently found in the center of the tumor. (B) A metastatic tumor nodule in lung. (C) Metastatic sites in liver. (D) Metastatic sites in spleen. (E) IHC for ERα of TA2 breast tumors. (F) IHC for PR of TA2 breast tumors. (G) IHC for HER-2 of TA2 breast tumors. TA2 breast cancers are negative for ER α, PR and HER-2. (H) Moderate expression of p53 is identified in TA2 breast tumors. (I) IHC for ALDH1 of TA2 breast tumors. (G) IHC for CD133 of TA2 breast tumors.
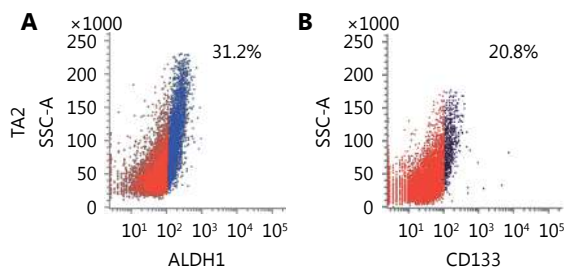

Figure S3 Isolation of ALDH1+ and CD133+ TA2 breast tumors cells. (A) FACS analyses of the ALDH1+ populations of TA2 breast tumors cells. (B) FACS analyses of the CD133+ populations of TA2 breast tumors cells.